Synthesis, Structure, and Properties of $Ca_{16}Sb_{11}$, a Complex Zintl Phase. Twelve Other Isotypic Compounds Formed by Divalent Metals and Pnictogens

E. Alejandro Leon-Escamilla, Weir-Mirn Hurng, Eric S. Peterson, and John D. Corbett*

Department of Chemistry and Ames Laboratory-DOE,[1] Iowa State University, Ames, Iowa 50011

Received August 22, 1996[⊗]

The systems A = Ca, Sr, Ba, Eu, Yb and Pn = As, Sb, Bi form isostructural $A_{16}Pn_{11}$ phases for all but Ba−As and Yb−As when the elements are reacted in Ta containers at about 1100 °C and then annealed at 825−900 °C or slowly cooled. It is important to run particularly the $Ae_{16}Sb_{11}$ reactions for Ae = Ca, Sr, Ba either under dynamic vacuum or to previously remove the pervasive hydrogen impurity from these metals. The tetragonal structure type was defined for $Ca_{16}Sb_{11}$ ($P\bar{4}2_1m$, $Z = 2$, $a = 12.253(3)$ Å, $c = 11.313(4)$ Å). The complex structure is built of pairs of confacial W_5Si_3-like slabs intergrown with single square-prismatic slabs along $\vec{c}$ in which Ca atoms in both define the polyhedra centered by Sb. This structure is the missing $n = 2$ member of the homologous series $A_{5n+6}B_{3n+5}$ (Parthé) with n:1 ratios of intergrown slabs. Four of five $Ae_{16}(Sb,Bi)_{11}$ examples studied are diamagnetic ($Ba_{16}Sb_{11}$ excepted), and $Ca_{16}Sb_{11}$ is a poor semiconductor. Accommodation of these Zintl-phase characteristics in the $Ca_{16}Sb_{11}$ structure requires that 50% of the Sb atom pairs centering the confacial square antiprisms be bonded ($d = 3.40$ Å) on a random basis. Ellipsoids on these atoms are elongated along the proposed bonds.

Introduction

Some seemingly simple and well-studied binary systems can be surprisingly incomplete and complex in detail. The Ca−Sb system illustrates these difficulties well as do the other alkali-earth metal Ae−pnictogen Pn systems (Ae = Ca, Sr, Ba; Pn = As, Sb, Bi). In the region around 40% at. % Pn, the Ae_5Pn_3 phases (37.5 at. % Pn) with the common Mn_5Si_3-type hexagonal structure are most familiar.[2,3] We have earlier established that the orthorhombic Yb_5Sb_3-type polymorph reported for Ca_5Sb_3 as well as seven other reported isotypes are in fact all hydrides, Ca_5Sb_3H, etc.[4,5] Several interstitial derivatives of the Ae_5Pn_3 phases have also been made and characterized as Zintl phases, e.g., Ca_5Sb_3Cl and Ca_5Sb_3F.[6] Interestingly, several unsuccessful attempts to introduce other elements into the Ca_5Sb_3 host were observed to produce instead the corresponding binary calcium-interstitial compound together with compositions near Ca_3Sb_2 (40 at. % Sb) that all had the same unknown powder pattern. Furthermore, this new pattern was of a single phase as it could be completely indexed with a primitive tetragonal cell.[7] There was no precedent for either the composition or the symmetry. A Ca_3Sb_2 composition was once proposed on the basis of thermal analysis, but this phase was after some time correctly assigned to hexagonal Ca_5Sb_3.[8−11] Several cubic $Ae_4Pn_{2.67}$ compounds (inverse-Th_3P_4-type and presumably substoichiometric, 40.0 at. % Pn) have been reported for divalent Eu or Yb,[2,3] and we have found others. The next but somewhat more distant possibility (47.6 at. % Pn) could be the related body-centered tetragonal $Ae_{11}Pn_{10}$ compounds ($Ho_{11}Ge_{10}$-type). These have, beyond $Ca_{11}Sb_{10}$ and $Ca_{11}Bi_{10}$,[12] been reported only for pnictides of Eu and Yb among the dipositive metals,[13−15] but these structures have distinctly longer c axes than the unknown noted above.

The present article reports the results of an extended study of this new phase, $Ca_{16}Sb_{11}$ (40.7 at. % Sb) and its many analogues. Structural studies have revealed problems with the crystallography as well as the bonding insofar as the close-shell configuration of the expected Zintl phase. (Isolated Sb anions would leave the phase just one electron short, $16\cdot2-11\cdot3 = -1$). In fact, $Ca_{16}Sb_{11}$ is diamagnetic, semiconducting, and a proper Zintl phase. Extension of the explorations beyond $Ae_{16}Pn_{11}$ to include the dominantly divalent Eu and Yb has shown that all told 13 of the 15 systems form isotypic $A_{16}Pn_{11}$ phases. Particular attention has been paid to ascertaining whether hydrogen, which is such a common impurity in commercial grade alkaline-earth metals, plays a significant role in the formation of these $A_{16}Pn_{11}$ compounds as it does with many other phases.

Experimental Section

Syntheses. All reactions were run on ∼250 mg scales in welded $^1/_4$ in. diameter Ta tubing using glovebox and other customary techniques. Reagents employed were sublimed Ca, Sr, Ba (APL Eng. Mater.), Y, La, Eu, and Yb (Ames Lab, >4-9's total), As (Aldrich (6-9's), Sb (AESAR, 5-9's), Bi (ORNL, reactor grade) and H_2 (Matheson, 5-9's). Welded Ta reaction containers and glovebox

[⊗] Abstract published in *Advance ACS Abstracts,* January 15, 1997.
(1) This research was supported by the Office of the Basic Energy Sciences, Materials Sciences Division, U.S. Department of Energy. The Ames Laboratory is operated by DOE by Iowa State University under Contract W-7405-Eng-82.
(2) *Binary Alloy Phase Diagrams,* 2nd ed.; Massalski, T. B., Ed.; ASM International: Materials Park, OH, 1990.
(3) Villars, P.; Calvert. L. D. *Pearson's Handbook of Crystallographic Data for Intermetallic Phases,* 2nd ed.; American Society for Metals International: Metals Park, OH, 1991.
(4) Leon-Escamilla, E. A.; Corbett, J. D. *J. Alloys Compd.* **1994**, *206*, L15.
(5) Leon-Escamilla, E. A.; Corbett, J. D. Unpublished research.
(6) Hurng, W.-M.; Corbett, J. D. *Chem. Mater.* **1989**, *1*, 311.
(7) Hurng, W.-M., Ph.D. Dissertation, Iowa State University, 1988.
(8) Kubaschewski, O.; Walter, A. *Z. Electrochem.* **1939**, *45*, 732.
(9) Brauer, G.; Müller, O. *Angew. Chem.* **1961**, *73*, 169.
(10) Martinez-Ripoll, M.; Brauer, G. *Acta Crystallogr.* **1974**, *30*, 1083.
(11) Bruzzone, G.; Franceschi, E.; Merlo, F. *J. Less-Common Met.* **1978**, *60*, 59.
(12) Deller, K.; Eisenmann, B. *Z. Anorg. Allg. Chem.* **1976**, *425*, 104.
(13) Clark, H. L.; Simpson, H. D.; Steinfink, H. *Inorg. Chem.* **1970**, *9*, 1962.
(14) Schmelczer, R.; Schwarzenbach, D.; Hulliger, F. *Z. Naturforsch.* **1979**, *34B*, 1213.
(15) Taylor, J. B.; Calvert, L. D.; Wang, Y. *J. Appl. Crystallogr.* **1979**, *12*, 249.

S0020-1669(96)01035-X CCC: $14.00

techniques for handling reactants and products have been described before.[6,16] The pervasive hydrogen impurities in the alkaline-earth metals[17] can be removed by heating them while sealed in Ta in high vacuum to 100−200 °C below the respective melting points for 8−24 h, depending on the quantity. Hydrogen readily passes through the walls of the Ta container above about 550 °C. These conditions were derived experimentally following consideration of the Ae−AeH_2 phase diagrams and H_2 dissociation pressures.[18] Removal of substantially all of the hydrogen can be readily perceived by the absence of a pressure surge when the temperature of the system is raised by 10−20 °C.

The effects of hydrogen on the systems investigated were studied, and assurances that adventitious hydrogen was not a factor or necessary were gained, with techniques already developed for the investigation of compounds of the alkaline-earth metals with Mn_5Si_3- and Cr_5B_3-type structures.[4,5] Ordinarily, Ta reaction containers are heated in evacuated and sealed fused silica jackets for protection of the former from the atmosphere during heating. Hydrogen contamination is known to occur by reduction of water that is slowly evolved from these jackets, depending particularly on the temperature and reaction period as well as, of course, the stability of the hydride product. Such reactions will be designated as sc (sealed container). Washing the SiO_2−Ta assembly with Ta cleaning solution (aq HF−HNO_3−H_2SO_4) and rinsing with deionized H_2O before evacuation together with strong flaming of the jacket while under high vacuum and before sealing were also routinely applied. The best assurance of maximum hydrogen removal is obtained by maintaining the Ta container under dynamic vacuum, marked as dv, at $\leq\sim10^{-5}$ torr during the entire reaction period. Hydrogen removal in this way can also avoid the necessity for prior cleaning of the alkaline-earth metals as well as Eu and Yb, although the latter do not generally present this problem.

As before, high-resolution Guinier powder patterns (Enraf-Nonius FR552) were employed throughout to analyze product purities, sort out mixtures, and identify unknowns. Powder patterns calculated for phases with known structures and printed on the same scale as the films were the usual process for phase identification. Known patterns were read and digitalized by a line scanner (LS20, KEJ Instruments, Stockholm), including the 4 or 5 lines of standard Si (NIST) added as an internal standard. Lattice constants of known phases were established by least-squares means from the film data for at least 30 reflections with known indices. Even traces of the red Ca_4Sb_2O were easily recognized visually.

Crystal Structure of $Ca_{16}Sb_{11}$. Several unknown patterns secured for compositions near Ca_3Sb_2 could be completely indexed by TREOR[19] (20−46 lines) with a primitive tetragonal cell, $a = b \cong 12.24$ Å, $c \cong 11.32$ Å. The cell type and size was very reminiscent of W_5Si-type structures with comparable *a* and *c*/2 axes, and a powder pattern calculated on such a basis showed a large resemblance to the experimental one. A family of compounds with compositions $A_{5n+6}B_{3n+5}$ that are based mainly on W_5Si_3-like building blocks was also noted.[20] The unknown $n = 2$ member $A_{16}B_{11}$ appeared to be a possible solution for our observations, and the $n = 5$ member $Ca_{31}Sn_{20}$[21] had a particularly similar *a* dimension. However, attempts to model a structure on the basis of this assignment and the expected space group[22] proved incomplete, and the detailed structure was solved by direct methods. The $n = 2$ assignment remained correct.

Several data sets were collected and refined to confirm the cell, space group, composition, and several unusual features of the structure. The structure was initially solved in the acentric space group $P\bar{4}2_1m$ by direct methods (SHELXS[23]) with data collected from a crystal of marginal size (6.3 reflections/variable). Later, crystals of better size were examined via overexposed Weissenberg and precession methods (4 and 3 days, respectively) for the *0kl* and *hk0* nets (and for corresponding second and third levels) without seeing any violations of the *0k0*, $k = 2n$, conditions or evidence for another or, particularly, a larger cell. Data from one of these were collected at room temperature on a CAD4 diffractometer with the aid of Mo Kα radiation to $2\theta = 54.9°$ and refined with the aid of the TEXSAN package.[24] The reflection statistics again clearly suggested a noncentrosymmetric cell. Some information is given in Table 1. Absorption was initially corrected by the average of two ψ-scans and later, after isotropic refinement, by DIFABS,[25] as recommended. After final convergence (R(F), $R_w = 2.7$, 3.3%), the enantiomeric choice was confirmed first by examination of $F_o - F_c$ values for weak reflections for which the choice made the larger differences and second by inverting the coordinates in the final refinement stages. The distinction with each was clear but small in effect. The final positional and isotropic-equivalent data are given in Table 2. More crystallographic and refinement data and the anisotropic displacement parameters are contained in the Supporting Information. These and the F_o/F_c listing are also available from J.D.C.

Table 1. Crystallographic Data for $Ca_{16}Sb_{11}$

fw	1980.5
space group, *Z*	$P\bar{4}2_1m$ (No. 113), 2
lattice params[a]	
a (Å)	12.253(3)
c (Å)	11.313(4)
V (Å^3)	1698.5(8)
ρ_{calcd} (g/cm^3)	3.873
absorp coeff (cm^{-1}, Mo Kα)	110.2
R/R_w[b] (%)	2.7/3.3

[a] Lattice parameters calculated from Guinier powder data, $\lambda = 1.540\,562$ Å, 22 °C. [b] $R = \sum||F_o| - |F_c||/\sum|F_o|$; $R_w = [\sum w(|F_o|^2 - |F_c|)^2/\sum w(F_o)^2]^{1/2}$; $w = \sigma_F^{-2}$.

Table 2. Positional Parameters and Isotropic Equivalent Displacement Parameters for $Ca_{16}Sb_{11}$ ($P\bar{4}2_1m$)

atom		*x*	*y*	*z*	B_{eq}[a]
Sb1[b]	4*d*	0	0	0.4698(1)	2.11(8)
Sb2	4*d*	0	0	0.150 37(7)	1.60(3)
Sb3	4*e*	0.373 08(4)	$x + 1/2$	0.486 75(7)	1.37(2)
Sb4	4*e*	0.355 02(4)	$x + 1/2$	0.031 73(7)	1.35(2)
Sb5	4*e*	0.179 25(4)	$x + 1/2$	0.762 10(6)	1.02(2)
Sb6	4*e*	0.163 98(4)	$x + 1/2$	0.236 49(6)	0.96(1)
Ca1	2*c*	0	1/2	0.7858(3)	1.24(8)
Ca2	2*c*	0	1/2	0.1401(3)	1.65(8)
Ca3	4*e*	0.1313(2)	$x + 1/2$	0.5010(2)	2.10(6)
Ca4	8*f*	0.2922(1)	0.5881(1)	−0.0010(1)	1.27(6)
Ca5	8*f*	0.4239(1)	0.7097(1)	0.2882(2)	1.53(7)
Ca6	8*f*	0.0706(1)	0.2032(2)	0.3159(2)	2.68(9)

[a] $B_{eq} = (8\pi^2/3)\sum_i\sum_j \mathbf{U}_{ij}a_i^*a_j^*\vec{a}_i\vec{a}_j$; Å^2. [b] Split position, 50% occupancy.

The refined ellipsoids for 4 or 5 atoms were found to be elongated with aspect ratios of 2.5:1−4:1, and these were characteristically about the same with all data sets. Explorations of subgroups of $P\bar{4}2_1m$ were carried out, particularly those obtained when symmetry elements that could be causing the pathological ellipsoidal behaviors were removed, but retaining when possible the strongly supported absence condition and *mmm* symmetry. Among the space groups so explored were $P42_12$, $P\bar{4}m2$, $P\bar{4}2c$, $P2_12_12$, $P2_122$, $P2_1/m$, $P2_1$, and triclinic. In no case was any of the seemingly problem ellipsoids significantly altered, and many refinements with lower symmetry were badly coupled or unstable.

Resistivity Measurements: Gram quantities of finely powdered $Ca_{16}Sb_{11}$ were pelletized (without binder) in a 1/4 inch d. SPECAC IR press within the glovebox. The very brittle pellets were carefully removed and annealed at 550−750 °C for 8−10 days while sealed within Ta or Nb containers. The dc conductivity was measured in a homemade four-

(16) Zhao, J.-T.; Corbett, J. D. *Inorg. Chem.* **1995**, *34*, 378.
(17) Peterson, D. T. *J. Met.* **1987**, *39*, 20.
(18) Magee, C. B. In *Metal Hydrides*; Mueller, W. M., Blackledge, J. P., Libowitz, G. G., Eds.; Academic Press: New York, 1968; Chapter 6.
(19) Werner, P. E. *TREOR-4 Trial and Error Program for Indexing Unknown Powder Patterns*; Department of Structural Chemistry, Arrhnius 20. Laboratory, University of Stockholm: S-106 91 Stockholm, Sweden, 1984.
(20) Leroy, J.; Moreau, J. M.; Paccard, D.; Parthé, E. *J. Less-Common Met.* **1980**, *76*, 131.
(21) Fornasini, M. L.; Franceschi, E. *Acta Crystallogr.* **1977**, *B33*, 3476.
(22) Yarmolyuk, Y. P.; Grin′, Y. N.; Olesh, O. M. *Sov. Phys.-Crystallogr.* **1980**, *25*, 143.
(23) Sheldrick, G. M. *SHELXS-86*; Universität Göttingen: Germany, 1986.
(24) *TEXSAN*, version 6.0. Molecular Structure Corp.: The Woodlands, TX 1990.
(25) Walker, N.; Stuart, D. *Acta Crystallogr.* **1983**, *A39*, 159.

Table 3. Typical Reactions Producing $Ca_{16}Sb_{11}$ and Its Lattice Constants (Å)

loaded composition[a]	reaction conditions[b]	product distribution[c]	*a*	*c*	*V* (Å^3)	*c*/*a*
$Ca_{16}Sb_{11}$[d]	i, sc	~100% $Ca_{16}Sb_{11}$	12.2641(1)	11.2966(8)	1699.1(1)	0.921
$Ca_{16}Sb_{11}$[e]	ii, sc	~95−98% $Ca_{16}Sb_{11}$, Ca_4Sb_2O	12.253(3)	11.313(4)	1698.5(8)	0.923
$Ca_{16}Sb_{11}$	i, dv	~100% $Ca_{16}Sb_{11}$	12.2332(4)	11.3463(6)	1698.0(1)	0.927
$Ca_{16}Sb_{11}$	i, sc	~80% $Ca_{16}Sb_{11}$, ~15% Ca_5Sb_3H, Ca_4Sb_2O	12.266(2)	11.288(3)	1698.3(5)	0.920
$Ca_{16}NaSb_{11}$	ii, dv	~95% $Ca_{16}Sb_{11}$, $NaSb_x$, Ca_4Sb_2O	12.348(1)	11.106(1)	1693.4(3)	0.899
$Ca_{15}YSb_{11}$	iii, dv	~60% $Ca_{16}Sb_{11}$, ~40% anti-Th_3P_4	12.2328(9)	11.347(2)	1698.0(4)	0.928
$Ca_{15}LaSb_{11}$	ii, sc	~40% $Ca_{16}Sb_{11}$, ~45% Ca_5Sb_3H, ~15% La	12.306(1)	11.235(2)	1701.4(4)	0.913
$Ca_{15}LaSb_{11}$	iii, dv	~100% Mn_5Si_3	9.0449(5)	7.0194(8)	497.32(8)	0.776

[a] Generally, Ca metal as received was used unless otherwise noted. [b] Conditions: (i) 1100 °C for 2 h, 10 °C/h to 650 °C. (ii) 1100 °C for 2−4 h, 20 °C/h to 850 °C, annealed for 8−15 days. (iii) 1300 °C for 4 h, then ~15 °C/h to 650 °C. sc = reaction with a sealed fused silica jacket. dv = reaction under dynamic vacuum. [c] By structure type, estimated from Guinier powder patterns. [d] Previously dehydrogenated Ca used. [e] A hydride-poorer Ca sample (Ames Lab) used as received.

probe apparatus.[26] The sample was held within a plastic plate and on a ceramic temperature indicator. Current contacts were positioned on opposed sides of the pellet and fed by a constant current source, while pogo-type gold-plated voltage contacts were placed in a colinear manner on the large face of the pellet. This assembly was loaded within a He-filled glovebox and sealed within a +-shaped, 3 cm i.d. stainless steel vacuum unit (Varian) capped by four vacuum flanges to provide good thermal mass. Data were collected on warming after the apparatus had first been immersed in liquid N_2.

Magnetic Susceptibilities. Weighed samples were loaded in the glovebox and held between two glass rods inside a 5 mm o.d. SiO_2 tube which was then sealed under He.[27] Magnetizations were measured between 6 and 300 K at a field of 3 T with a Quantum Design MPMS SQUID magnetometer. The raw data were corrected for the sample holder and for the diamagnetic atom cores.

Results and Discussion

$Ca_{16}Sb_{11}$. Reactions between calcium and antimony at the proper stoichiometry at 1100 °C followed by slow cooling or annealing at 850−900 °C gave quantitative yields according to Guinier patterns. Table 3 shows the results of selected reactions carried out under various conditions. The effect of impurity hydrogen in this system can be recognized in the fourth reaction, where the ternary orthorhombic Ca_5Sb_3H (Ca_5Sb_3F-type[6]) formed in lesser amounts when commercial Ca was used as the reagent and the welded tantalum tube was sealed in a fused silica container (sc) from which H_2O slowly evolves. When the reaction container was heated under dynamic vacuum (dv, hydrogen-free) conditions, $Ca_{16}Sb_{11}$ was the only product, and the tetragonal *a* and *c* dimensions were ~0.03 Å smaller and ~0.06 Å larger, respectively, than before (third reaction, Table 3). Smaller differences were generally found when there was less hydrogen contamination, such as in reactions loaded with clean or better quality Ca but run in the sealed silica jacket (first two examples, Table 3). The cell volumes among these products are not significantly different.

Unusual features of the $Ca_{16}Sb_{11}$ structure (below) were originally interpreted in terms of electron-imprecise (nonZintl) characteristics, and so a diversity of reactions intended to vary the electron count in this structure were attempted through doping with third elements. None gave the desired ordered structure. Thus, compositions intended to reduce the electron concentrations, $Ca_{16-x}(Na,K)_xSb_{11}$, $x = 1$, 2, led to a tetragonal phase initially identified as $Ca_{11}Sb_{10}$ in the $Ho_{11}Ge_{10}$-type structure (*I*4/*mmm*[12]) and believed to be the sodium- or potassium-substituted version, $Ca_{11-x}(Na,K)_xSb_{10}$. However, subsequent experimental efforts demonstrated this to be a new binary in the Ca−Sb system with a composition near $Ca_{11}Sb_9$ ($P\bar{4}_2/mmm$), a defect variation of $Ca_{11}Sb_{10}$.[28] The two structures cannot be easily differentiated by powder data without exceptional quality Guinier patterns.

Some reactions intended to give electron-richer products did give $Ca_{16}Sb_{11}$-like patterns. Those that involved additional sodium, like $Ca_{16}NaSb_{11}$, gave products with distinctly larger *a* and smaller *c* axes, and volume decrements of ~0.33% (Table 3). Attempted refinement of the structure gave greater Ca displacement anisotropies than for the binary structure, but no new positions were generated, so partial substitution of Ca by Na appeared probable, and the problem was abandoned when the structure could not be refined well. Reactions targeted at substitution by rare-earth metals Y or La did not achieve the expected structural ordering. Reactions heated to 1100 °C and below were incomplete, while those heated at 1300 °C under vacuum conditions gave apparently unchanged $Ca_{16}Sb_{11}$ plus an inverse Th_3P_4-type phase with Y and a substituted Mn_5Si_3-type structure with La.

Other $A_{16}Pn_{11}$ Systems. The formation of phases with the $Ca_{16}Sb_{11}$ structure type was further explored for A = Ca, Sr, Ba, Eu, Yb and Pn = As, Sb, Bi following the approach used in our earlier studies of analogous A_5Pn_3 (Mn_5Si_3-type) and A_5Pn_3H (Ca_5Sb_3F-type) systems.[4] Most were carried out with as-received metals in Ta containers under both dynamic vacuum and sealed tube conditions in order to assess the role of hydrogen impurities, while more hydrogen was added to a few reactions as AH_2. No further case of the formation of a $A_5Pn_3(H)$ phase was encountered in this set of systems.

All combinations except Ba−As and Yb−As produce isostructural gray to black $A_{16}Pn_{11}$ compounds, Table 4. As before, a few $A_{16}Pn_{11}$ phases exhibited smallish perturbations of the cell dimensions (*a* smaller, *c* larger) when the reaction was run in a sealed silica jacket or AH_2 was added, namely $Sr_{16}Sb_{11}$, $Ba_{16}Sb_{11}$, and possibly $Eu_{16}As_{11}$ (Table 4). The others did not seem to be so influenced. A second, lower symmetry Ca−Bi phase that is similar in composition to $Ca_{16}Bi_{11}$ was obtained in an evacuated system after slow cooling from 1100 to 650 °C rather than annealing at 900 °C (Table 4). Its structure could not be solved completely with the small crystals available.[28] The two absent $A_{16}Pn_{11}$ combinations form the cubic anti-Th_3P_4 structure or a distorted version instead. The cubic structure was additionally seen for Sr−Bi, Ba−Bi, Eu−Bi, Yb−As, Yb−Sb, and Yb−Bi systems, more so in sealed tube reactions. Their stoichiometries would be close to the $A_{16}Pn_{11}$ phases sought if the expected (but not always found) valence-precise compositions $A_4Pn_{2.67}$ (A_3Pn_2) pertain.[28,29]

The $Ca_{16}Sb_{11}$ Structure. This is remarkable in both its complexity and the implications of unusual, disordered Sb−Sb bonding that make it a valence compound. Therefore, the structure was studied for three independent samples to establish

(26) Wolfe, L. G. M. S. Thesis, Iowa State University, 1990.
(27) Guloy, A. M.; Corbett, J. D. *Inorg. Chem.* **1996**, *35*, 4669.
(28) Leon-Escamilla, E. A. Ph.D. Dissertation, Iowa State University, 1996.
(29) Wang, Y.; Calvert, L. D.; Taylor, J. B. *Acta Crystallogr.* **1980**, *B36*, 221.

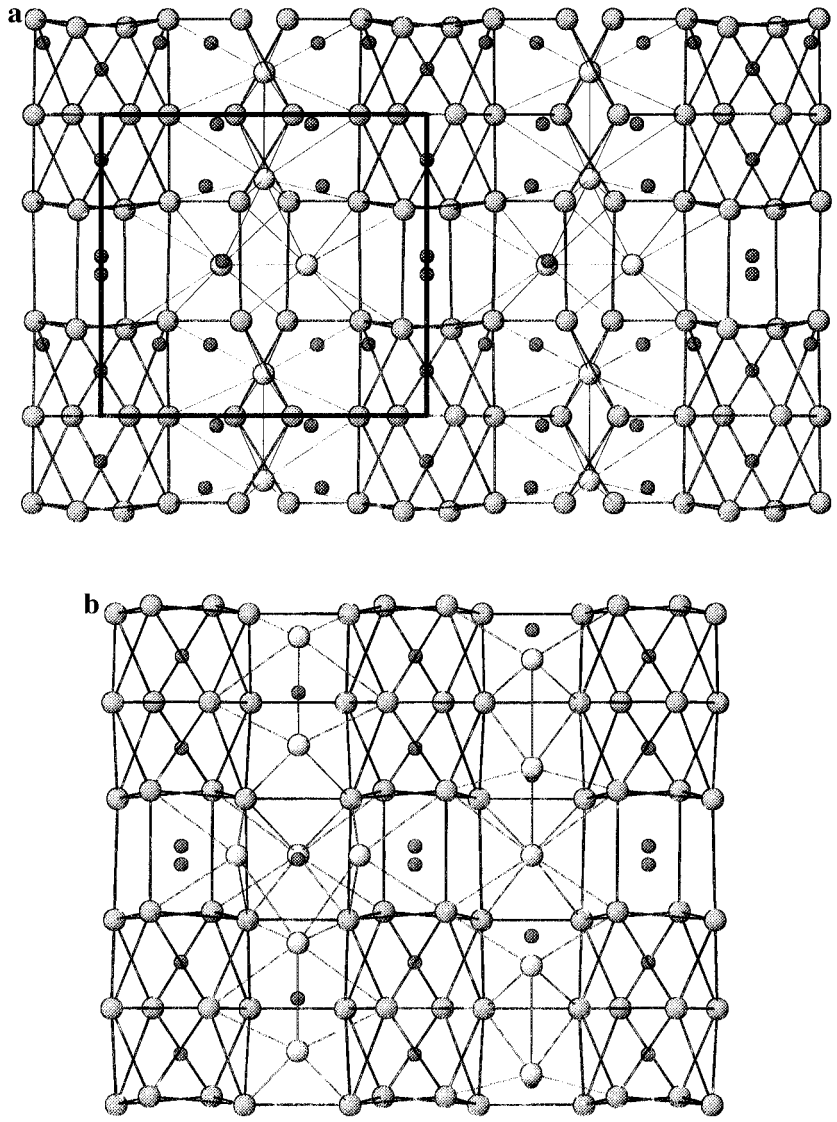

Figure 1. Structure of $Ca_{16}Sb_{11}$: (a) 010 section with the cell face outlined; $\vec{c}$ vertical. The smaller dark spheres represent antimony. Lines between calcium atoms only emphasize geometric features, the heavier lines highlighting the columns of confacial square-prismatic and -antiprismatic calcium polyhedra that distinguish this structure type. (b) Comparable 110 section with calcium polyhedra outlined. The horizontal slabs are defined by pairs of square antiprisms containing Sb2 and a complex figure centered by Sb4, while central slab contains Sb1 (split) and Sb3 atoms.

that there was no detectable superstructure or alternate cell, that the ellipsoidal behavior of some atoms were characteristic, not accidental, and that the structure did not depend on, or change with, the presence of hydride or other impurities. The structure reported here is that with the lowest positional errors and the smallest isotropic-equivalent ellipsoids. That obtained with a crystal from a hydrogen-free (dv) synthesis (Table 3) had slightly higher errors, a little larger isotropic ellipsoids, and the anisotropic ellipsoids of the four generally problematic atoms were slightly more extreme. Otherwise, the results were equivalent. Details on assurances that the results pertain to the correct cell, space group and enantiomer are given in the Experimental Section.

The positional and isotropic displacement parameters for $Ca_{16}Sb_{11}$ are listed in Table 2. A 010 section of the rather complex structure is shown in Figure 1a with the cell outlined to emphasize the stacking sequences, while Figure 1b shows the 110 view. The 001 projection of the structure along the 11.3 Å *c* axis is shown in Figure 2. Lines between cations in both figures are drawn only to provide geometric reference for the calcium polyhedra, with the characteristic, square prism−antiprism columns given a heavier outline in Figure 1a. (A perspective view of one cell face with the atom numbering scheme to aid in the orientation of later polyhedral descriptions is given in the Supporting Information.) The distinctive vertical columns in Figure 1, seen in projection along 0,0,*z* and $^1/_2$,$^1/_2$,*z* in Figure 2, contain a confacial stacking of (intergrowth between) pairs of square antiprisms of Ca about Sb2 with one square prism (cube) of cations around the split Sb1 site. One of these columns is shown isolated in Figure 3 with its characteristic ellipsoid pattern. This square prism−antiprism pattern serves to place this structure within a homologous series of related structures (below). The larger complex regions that intervene along 0, $^1/_2$, *z*, etc. (Figures 1a and 2) contain Sb3, 4, 5, and 6 atoms within calcium polyhedra, all with *m* symmetry. Those along *c* in the 110 section (Figure 1b, left) are clearer, a 10-atom polyhedra about Sb4 (top) and a distorted square antiprism about Sb3.

The polyhedra about each of the antimony atoms are illustrated in Figure 4, and those about each calcium are shown in Figure 5. (The unsplit Sb1 centroid is shown in the latter.) The polyhedra are oriented so as make the shapes clear, and not along any particular crystallographic direction. Important distances in the structure are given in Table 5. Although "normal" Ca−Sb distances fall in a range about 3.05−3.4 Å, separations greater than 4.00 Å have been included about Sb3,

Table 4. $Ca_{16}Sb_{11}$-Type Reaction Products in Other $A_{16}Pn_{11}$ Systems and Their Lattice Constants (Å)

loaded composition[a]	reaction conditions[b]	product distribution[c]	*a*	*c*	*V* (Å^3)	*c*/*a*
$Ca_{16}As_{11}$	i, dv/sc	~90%, un	11.686(3)	10.511(3)	1435.4(6)	0.899
$Ca_{16}Bi_{11}$	i, dv/sc	~95%, un	12.4949(8)	11.430(1)	1784.5(2)	0.915
$Sr_{16}As_{11}$	i, dv/sc	~90%, un	12.2954(4)	11.1598(8)	1687.1(2)	0.908
$Sr_5As_3H_2$	iii, sc	~95%, un	12.2959(7)	11.159(2)	1687.2(3)	0.907
$Sr_{16}Sb_{11}$	iii, sc	~100%	12.9115(5)	11.8343(8)	1972.8(2)	0.917
$Sr_{16}Sb_{11}$	iv, dv	~100%	12.9341(5)	11.8027(7)	1974.5(2)	0.912
$Sr_{16}Bi_{11}$	ii, dv/sc	~80%, ~20% ATP	13.157(2)	11.935(3)	2066.0(6)	0.907
$Sr_{16}Bi_{11}$	iv, sc	~95%, ~5% ATP	13.152(1)	11.934(2)	2064.2(5)	0.907
$Ba_{16}Sb_{11}$	iii, sc	~100%	13.570(2)	12.411(3)	2285.3(7)	0.915
$Ba_{16}Sb_{11}$	iii, dv	~100%	13.582(2)	12.393(4)	2286.3(9)	0.912
$Ba_{16}Bi_{11}$	v, dv	~40%, ~55% ATP, Ox	13.744(1)	12.568(1)	2374.2(4)	0.914
$Eu_{16}As_{11}$	i, dv/sc	~90%, un	12.0885(5)	11.040(1)	1613.3(3)	0.913
$Eu_5As_3H_2$	iv, sc	>95%, un	12.080(2)	11.054(3)	1613.1(6)	0.915
$Eu_{16}Sb_{11}$	v, dv	~100%	12.737(1)	11.668(2)	1892.9(3)	0.916
$Eu_{16}Bi_{11}$	v, dv	~85%, ~15% ATP	12.906(3)	11.852(6)	1974(1)	0.918
$Yb_{16}Sb_{11}$	iv, dv	~95%, ~5% ATP	12.1686(5)	11.320(1)	1676.2(2)	0.930
$Yb_{16}Bi_{11}$	iv, dv	~40%, ~60% ATP	12.3694(7)	11.588(1)	1766.9(2)	0.933

[a] Active metals used as received. [b] Conditions: (i) Vacuum; 1100 °C for 6 h, 15 °C/h to 850 °C, quenched. Annealed in sealed container at 900 °C for 30 d. (ii) Vacuum; 1100 °C for 36 h, 2 °C/h to 900 °C, held for 14 days, quenched. (iii) 1100 °C for 3 h, 15 °C/h to 825 °C, held for 10 d, quenched. (iv) 1100 °C for 3 h, 10 °C/h to 650 °C. (v) As in iv but 1150 °C. sc = reaction in a sealed fused silica container. dv = reaction under dynamic vacuum. [c] Percent $A_{16}Pn_{11}$ followed by other phases: ATP = anti-Th_3P_4 (cubic); Ox = Ca_4Sb_2O type (inverse K_2NiF_4; cubic); un = unknown.

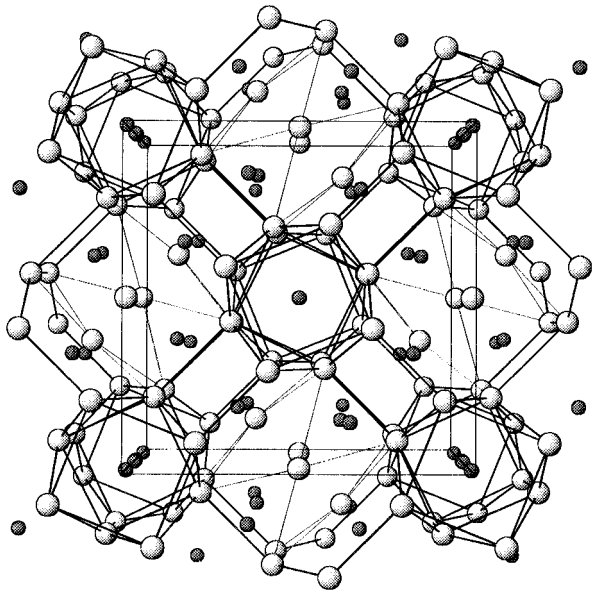

Figure 2. 001 projection of the structure of $Ca_{16}Sb_{11}$, with calcium polyhedra outlined. Small spheres are antimony atoms, with Sb1 unsplit.

Sb4, Ca2, Ca3, and Ca6 in the figures to better describe the polyhedron about each. Radial "bonds" are not drawn for these long distances, and they are not counted in the coordination numbers.

Figure 4 shows how the Sb3, Sb5, and Sb6 atoms are seven- or eight-coordinate in distorted mono- or bicapped trigonal prismatic polyhedra of calcium. The last two cavities are more restrictive, accounting for the smaller thermal ellipsoids for those atoms. The remaining Sb4 is eight-coordinate in a very low-symmetry arrangement, but a very distorted bicapped square prism can be found when the long Sb4−Ca6 separations included, the sequences Ca4−5−4−6 defining the square end faces. Among the cations, Ca1, 4, 5 are surrounded by distorted octahedra of antimony and, accordingly, have small isotropic ellipsoids, Figure 5. The other three cations give the impression of having relaxed off the centers of the surrounding antimony polyhedra to better bonding (coulombic) sites. Ca2 and Ca6 lie within distorted octahedra with four and five bonding neighbors, respectively, while Ca3 is four-bonded within some kind of a larger decahedron.

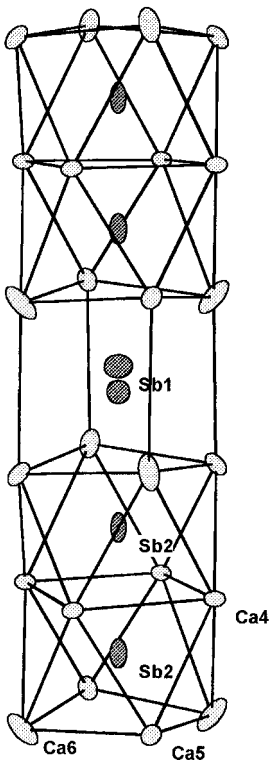

Figure 3. The characteristic square antiprism−prism column in $Ca_{16}Sb_{11}$ with independent atoms labeled (70% thermal ellipsoids).

The 50:50 splitting of the Sb1 site appears to result from the oversized, roughly square prismatic cavity afforded by Ca5 and Ca6, which can also be described as a pair of stellated tetrahedra, the Ca6 member being the smaller. The large but roughly spherical ellipsoids for each Sb1 component are also consistent with a more static, four-coordinate placement. Otherwise, the anisotropic displacement ellipsoids of all atoms are consistent with their environments and reproducible in shape characteristics from crystal to crystal. The extreme $\mathbf{U}_{ii}/\mathbf{U}_{jj}$ axial ratios for all antimony atoms are ≤2.1:1 except $U_{33}/U_{11} = 3.93$ for Sb2. The last appears significant in the bonding description (below). Extremes of 2.6−2.7 for U_{33}/U_{11} for Ca1 and Ca6 and 0.26 for Ca3 appear to result from the low symmetry of the surrounding polyhedra.

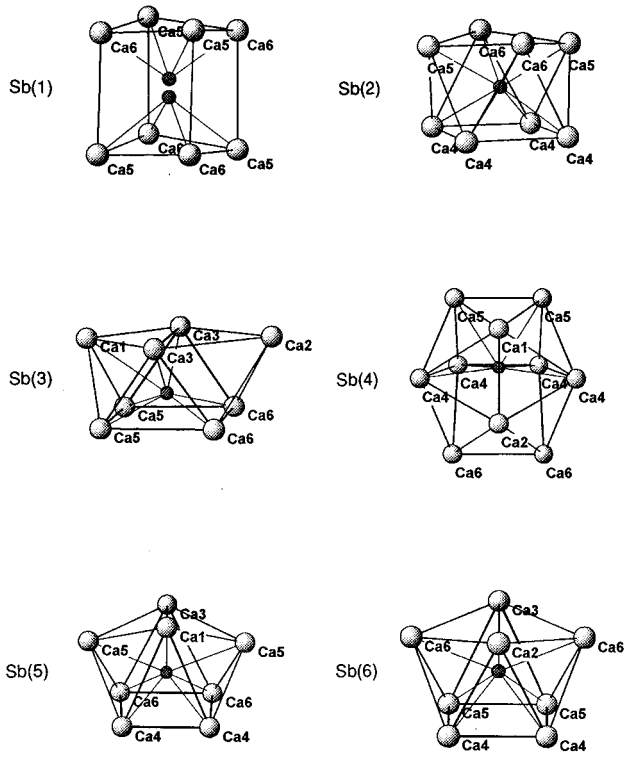

Figure 4. The calcium polyhedra about the individual antimony atoms (dark spheres) in the $Ca_{16}Sb_{11}$ structure. Radial Ca−Sb "bonds" are not drawn about Sb3 and Sb4 for separations >4.0 Å. Orientations are arbitrary.

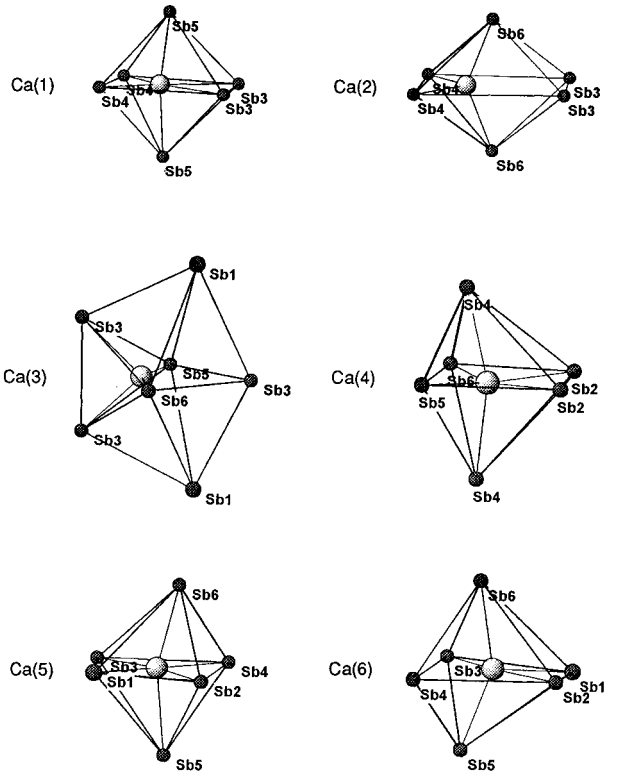

Figure 5. Antimony polyhedra about calcium atoms in $Ca_{16}Sb_{11}$. The Sb1 atoms are shown unsplit. Ca−Sb separations >4.00 Å about the distinctly off-center Ca2, 3, 6 are not marked by radial lines.

A Family of Structures. In spite of the somewhat intimidating character of this structure, Figures 1 and 2, the result fits nicely into a homologous series of structures. These are variously constructed from slabs based on either square-antiprismatic or square-prismatic coordination of various p elements by the active metal component. The phase compositions are given by $A_{5n+6}B_{3n+5}$ where n is the number of antiprism-based slabs between single slabs of square prisms (cubes).[20] The parent formula and the space group for each n-type are summarized in Table 6. The W_5Si_3 parent, $n = \infty$, is built only of slabs that contain W_8 square antiprisms centered by Si that are laterally separated by Si-centered W_{10} polyhedra. These stack in a confacial manner out the tetragonal c axis. The $n = 6$ member consists of six W_5Si_3-like slabs of centered square antiprisms intergrown with a single slab built around centered square prisms. This has recently been found in $Yb_{36}Sn_{23}$. The $n = 5$ parent is $Pu_{31}Pt_{20}$,[32] although $Ca_{31}Sn_{20}$ is more relevant here, $n = 4$ has a complex composition but the 4:1

Table 5. Interatomic Distances (Å) in $Ca_{16}Sb_{11}$

Sb1[a]−Ca5	(×2)	3.418(2)	Ca1−Sb3	(×2)	3.787(3)
Sb1−Ca5	(×2)	3.867(2)	Ca1−Sb4	(×2)	3.252(2)
Sb1−Ca6	(×2)	3.159(3)	Ca1−Sb5	(×2)	3.117(6)
Sb1−Ca6	(×2)	3.581(3)			
			Ca2−Sb3	(×2)	4.779(3)
Sb2−Ca4	(×2)	3.240(2)	Ca2−Sb4	(×2)	3.177(2)
Sb2−Ca4	(×2)	3.252(2)	Ca2−Sb6	(×2)	3.043(2)
Sb2−Ca5	(×2)	3.147(2)			
Sb2−Ca6	(×2)	3.232(2)	Ca3−Sb1	(×2)	4.807(2)[b]
					[4.808(2)][c]
Sb3−Ca1		3.787(3)	Ca3−Sb3	(×2)	3.168(2)
Sb3−Ca2		4.779(3)[b]	Ca3−Sb3		4.192(3)[b]
Sb3−Ca3	(×2)	3.168(2)	Ca3−Sb5		3.071(3)
Sb3−Ca5	(×2)	3.072(2)	Ca3−Sb6		3.043(3)
Sb3−Ca6	(×2)	3.131(2)			
Sb4−Ca1		3.252(2)	Ca4−Sb2		3.240(2)
Sb4−Ca2		3.177(2)	Ca4−Sb2		3.252(2)
Sb4−Ca4	(×2)	3.380(2)	Ca4−Sb4		3.380(2)
Sb4−Ca4	(×2)	3.397(2)	Ca4−Sb4		3.397(2)
Sb4−Ca5	(×2)	3.509(2)	Ca4−Sb5		3.217(2)
Sb4−Ca6	(×2)	4.444(3)[b]	Ca4−Sb6		3.043(2)
Sb5−Ca1		3.117(1)	Ca5−Sb1		3.418(2)
Sb5−Ca3		3.071(3)			[3.867(2)][c]
Sb5−Ca4	(×2)	3.217(2)	Ca5−Sb2		3.147(2)
Sb5−Ca5	(×2)	3.459(2)	Ca5−Sb3		3.072(2)
Sb5−Ca6	(×2)	3.203(2)	Ca5−Sb4		3.509(2)
			Ca5−Sb5		3.459(2)
Sb6−Ca2		3.043(2)	Ca5−Sb6		3.287(2)
Sb6−Ca3		3.043(3)			
Sb6−Ca4	(×2)	3.249(2)	Ca6−Sb1		3.159(3)
Sb6−Ca5	(×2)	3.287(2)			[3.581(3)][c]
Sb6−Ca6	(×2)	3.423(2)	Ca6−Sb2		3.232(2)
			Ca6−Sb3		3.131(2)
Sb1[a]−Sb1		0.683(3)	Ca6−Sb4		4.444(3)[b]
Sb1−Sb2		3.614(2)	Ca6−Sb5		3.203(2)
Sb1−Sb2		4.297(2)	Ca6−Sb6		3.423(2)
Sb2−Sb2		3.402(2)[d]	Ca4−Ca4		3.539(3)[d]

[a] Split position, 50% occupancy. [b] Atom included to complete the polyhedron. [c] Number in brackets corresponds to distance to the other split Sb1. [d] Other Sb−Sb and Ca−Ca separations are greater than 4.04 and 3.70 Å, respectively.

Table 6. The Family of Known $A_{5n+6}B_{3n+5}$ Compounds

n	compd (parent)	space group	a (Å)	c (Å)	ref
∞	Ca_5Pt_3 (W_5Si_3)	$I4/mcm$	11.563	5.753	30
2	$Ca_{16}Sb_{11}$	$P\bar{4}2_1m$	12.2332(4)	11.3463(6)	this work
3	$Y_{21}Rh_{14}$ (Y_3Rh_2)	$I4/mcm$	11.232(2)	25.16(1)	31
4	$Sm_{26}(Ga_{0.35}Co_{0.65})_{17}$	$P4/mbm$	11.713(4)	15.171(7)	22
5	$Ca_{31}Sn_{20}$ ($Pu_{31}Pt_{20}$)	$I4/mcm$	12.5267(5)	39.912(7)	21
6	$Yb_{36}Sn_{23}$	$P4/mbm$	12.3898(4)	22.901(1)	5

(30) Palenzona, A. *J. Less-Common Met.* **1981**, *78*, 49.
(31) Moreau, J. M.; Paccard, D.; Parthé, E. *Acta Crystallogr.* **1976**, *B32*, 1767.
(32) Cromer, D. T.; Larson, A. C. *Acta Crystallogr.* **1977**, *B33*, 2620.

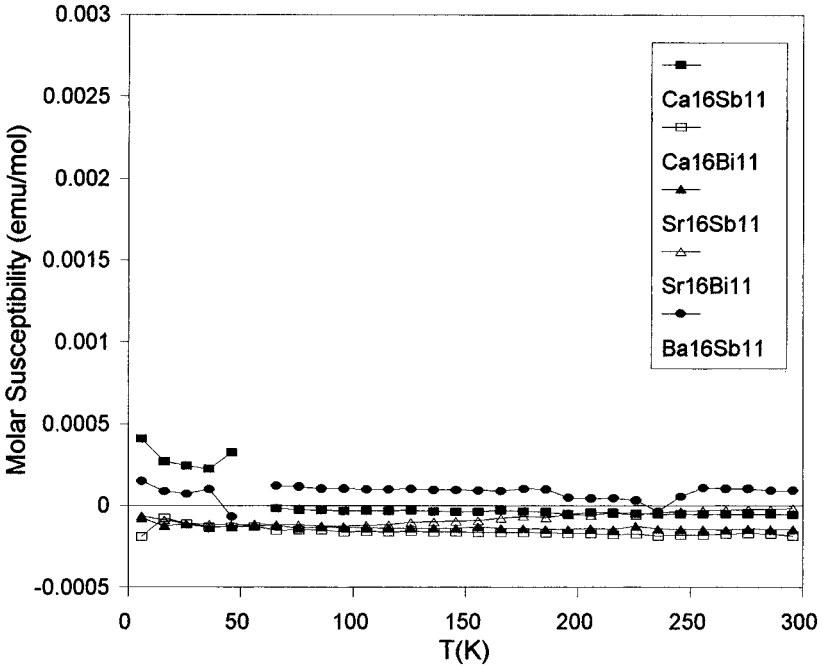

Figure 6. The molar magnetic susceptibilities of (bottom to top at 293 K) $Ca_{16}Bi_{11}$, $Sr_{16}Sb_{11}$, $Ca_{16}Sb_{11}$, $Sr_{16}Bi_{11}$, and $Ba_{16}Sb_{11}$ after core corrections. (The irregularities in two curves near 56 K were caused by condensation of oxygen on the exterior of the containers.)

slab stacking, $n = 3$ corresponds to Y_3Rh_2 ($Y_{21}Rh_{14}$), and $n = 2$ is the present $Ca_{16}Sb_{11}$. In fact, the last composition was recognized from the cell dimensions and Bravais lattice type before the structure was solved. Inspection of the figures will show that distortions and an altered composition are necessary where a W_5Si_3-type slab intergrows with a square prismatic (cube)-based slab, and a new eight-atom polyhedron appears in the former around Sb4.

Properties and Bonding. Conductivity and magnetic properties make clear that these $A_{16}Pn_{11}$ compounds should for the main part be viewed as valence compounds, i.e., Zintl phases. It has been noted before that structures of this complexity presumably reflect a considerable drive to accommodate closed-shell bonding. A pressed and annealed pellet of $Ca_{16}Sb_{11}$ measured by a four-probe null method over 213−293 K showed a sizable specific resistivity, $\rho_{273} \approx 3 \times 10^5\ \Omega$ cm, and $E_g = 0.46(2)$ eV over 253−293 K. The molar magnetic susceptibilities of five $Ae_{16}Sb_{11}$ phases, Ae = Ca, Sr, Ba and $Ae_{16}Bi_{11}$, Ae = Ca, Sr after core corrections are shown in Figure 6. These are all slightly negative (diamagnetic) over 60−300 K except for $Ba_{16}Sb_{11}$, which is weakly paramagnetic ($\chi \approx 1 \times 10^{-4}$ emu/mol).

The features of importance in understanding how the observed structure allows the fulfillment of closed-shell bonding lie in the antimony interactions. The important separations are Sb2−Sb2 through the W_5Si_3-like cell faces, 3.418(3) Å, and Sb1 (split)−Sb2, 3.617(3) Å (Figure 3). "Normal" single Sb−Sb bonds in the range 2.9−3.0 Å can be found in a variety of compounds, e.g., Sr_2Sb_3,[33] Ba_5Sb_4,[34] La_3TiSb_5,[35] while separations of 2.95−3.36 Å have been conceived as bonding distances in $Ca_{11}Sb_{10}$[12] and $Ba_7Ga_4Sb_9$.[36] But, we should not be too concerned about "normal" ranges in a structure such as this; matrix effects originating with closed-shell contacts of Sb2 with the cation structure (packing) are a likely reason why, for example, the Sb2−Sb2 approach is limited to 3.402(2) Å (center to center). Electron pairing (trapping) at room temperature is what we observe, and so we shall provisionally accept this length as suitable for a bona fide electron-pair bond. On the other hand, the Ca (5,6)−Sb1 distances and the fairly spherical Sb1 displacement figure certainly seem to support the notion that the Sb1 splitting is a result of an oversized cavity and not a competitive Sb1−Sb2 bonding at the longer 3.62 Å separation.

The bonding dilemma that remains is the following: the presence of only isolated Sb^{-3} states would leave the compound one electron short ($16Ca^{2+} \neq 11Sb^{3-}$) while a phase with all Sb2 atoms dimerized would be electron-rich and presumably metallic [$(Ca^{+2})_{16}(Sb^{-3})_9(Sb_2^{-4})e^-$]. Bonding between Sb1 (split)−Sb2 instead is equivalent. Trapping of delocalized electron pairs in some kind of multicenter cation sites would seem unlikely although it is not unprecedented, e.g., in Pr_2Br_5 apparently.[37] Organized fractional Sb−Sb bonding in some supercell, e.g., in $\vec{c}$, could solve the problem, but we have been unsuccessful in discerning any such ordered arrangement (Experimental Section). We are therefore forced to the conclusion that Sb2 pair bonding occurs in a spatially disordered manner, that is, with 50% Sb2−Sb2 electron pair bonds (one per cell) on a random basis. Note that the root-mean-square displacement corresponding to U_{33} for Sb2 is 0.77 Å, sufficient to give reasonable "normal" bond lengths. Involvement of the split Sb1 sites within the square prismatic cavities might also be considered, either in a bonding or repulsion mode, although the ellipsoids for split Sb1 no longer show elongation along $\vec{c}$ that would suggest any further disorder.

Single crystals of marginal size have also been examined structurally for $Eu_{16}As_{11}$, $Ca_{16}Bi_{11}$, and $Sr_{16}Bi_{11}$. These gave much less satisfactory refinements, largely because only 20−30% of possible reflections were observed. The best refinements were in the same space group as $Ca_{16}Sb_{11}$, but these exhibited similar pathologies with highly anisotropic or split positions for A1, A2, A3, A6, Pn1, and Pn2. We have also seen a phase near $Ca_{16}Bi_{11}$ in composition with only orthor-

(33) Eisenmann, B. *Z. Naturforsch.* **1979**, *34b*, 1162.
(34) Brechtel, E.; Cordier, G.; Schäfer, H. *Z. Naturforsch.* **1981**, *36b*, 1341.
(35) Bolloré, G.; Ferguson, M. J.; Hushagen, R. W.; Mar, A. *Chem. Mater.* **1995**, *7*, 2229.
(36) Cordier, G.; Schäfer, H.; Selter, M. *Z. Anorg. Allg. Chem.* **1986**, *534*, 137.
(37) Meyer, G.; Meyer, H.-J. *Chem Mater.* **1992**, *4*, 1163.

hombic symmetry, *a* and *b* differing by about 0.07 Å, but only partial refinement of the structure has been achieved.[28]

A surprising aspect of the present study is that these $A_{16}Pn_{11}$ phases exist in 13 of the 15 systems possible with A = Ca, Sr, Ba, Eu, Yb with Pn = As, Sb, Bi, yet no previous X-ray or thermal analysis evidence for any of these seems to have been reported. This may have been caused in many cases by the overwhelming effects of hydrogen impurities that seem to have been present in many of the earlier studies, particularly for Ca, Sr, Ba. Eight of the same systems studied here also form the very stable orthorhombic A_5Pn_3H phases (Ca_5Sb_3F-type),[4] which contain 37.5 at. % Pn among the heavy elements vs 40.7% Pn in $A_{16}Pn_{11}$. We have in fact observed the coexistence of orthorhombic Sr_5Sb_3H with $Sr_{11}Sb_{10}$ (or possibly $Sr_{11}Sb_9$, 45 at. % Sb), without the intervening $Sr_{16}Sb_{11}$, incidental to other experiments on the hydrides.[38] A recent report of the Ca−Sb system by thermal analysis and reaction calorimetry[39] again does not recognize $Ca_{16}Sb_{11}$, although they do include "Ca_2Sb" in their phase diagram, a phase that is known to be Ca_4Sb_2O instead (inverse K_2NiF_4 structure).[40] The newly identified peritectic decomposition at 996 °C might better be assigned to $Ca_{16}Sb_{11}$.

Finally, the role of the possibly substoichiometric anti-Th_3P_4-type $A_4Pn_{2.67}$[28,29] phases that could intervene in these systems is not at all clear. The proportion of this phase found after $A_{16}Pn_{11}$ syntheses appeared to increase for sc conditions in some, but not all, systems, suggesting that small amounts of H or O may be involved.

Acknowledgment. The resistivity data for $Ca_{16}Sb_{11}$ were kindly measured by Larry Wolfe, and the magnetic susceptibilities, by Jerome Ostenson.

Supporting Information Available: More details on the crystallographic study of $Ca_{16}Sb_{11}$ including anisotropic displacement parameters and a perspective view of the structure with the atoms labeled (3 pages). Ordering information is given on any current masthead page.

IC961035W

(38) The phases $Sr_{11}Sb_{10}$ and $Sr_{11}Bi_{10}$ have been newly identified.[28]

(39) Notin, M.; Mejbar, J.; Bouhajib, A.; Charles, J.; Hertz, J. *J. Alloys Compd.* **1995**, *220*, 62.

(40) Eisenmann, B.; Limartha, N.; Schäfer, H.; Graf, H. A. *Z. Naturforsch.* **1980**, *35b*, 1518.